NANO LETTERS

Letter

pubs.acs.org/NanoLett

Hybrid Surface-Phonon-Plasmon Polariton Modes in Graphene/Monolayer h-BN Heterostructures

Victor W. Brar,[†,‡,⊥] Min Seok Jang,[§,⊥] Michelle Sherrott,[†] Seyoon Kim,[†] Josue J. Lopez,[†] Laura B. Kim,[†] Mansoo Choi,[§,∥] and Harry Atwater*[,†,‡]

[†]Thomas J. Watson Laboratory of Applied Physics and [‡]Kavli Nanoscience Institute, California Institute of Technology, Pasadena, California 91125, United States

[§]Global Frontier Center for Multiscale Energy Systems, Seoul National University, Seoul 151-747, Republic of Korea

[∥]Division of WCU Multiscale Mechanical Design, School of Mechanical and Aerospace Engineering, Seoul National University, Seoul 151-742, Republic of Korea

Supporting Information

ABSTRACT: Infrared transmission measurements reveal the hybridization of graphene plasmons and the phonons in a monolayer hexagonal boron nitride (h-BN) sheet. Frequency-wavevector dispersion relations of the electromagnetically coupled graphene plasmon/h-BN phonon modes are derived from measurement of nanoresonators with widths varying from 30 to 300 nm. It is shown that the graphene plasmon mode is split into two distinct optical modes that display an anticrossing behavior near the energy of the h-BN optical phonon at 1370 cm^{-1}. We explain this behavior as a classical electromagnetic strong-coupling with the highly confined near fields of the graphene plasmons allowing for hybridization with the phonons of the atomically thin h-BN layer to create two clearly separated new surface-phonon-plasmon-polariton (SPPP) modes.

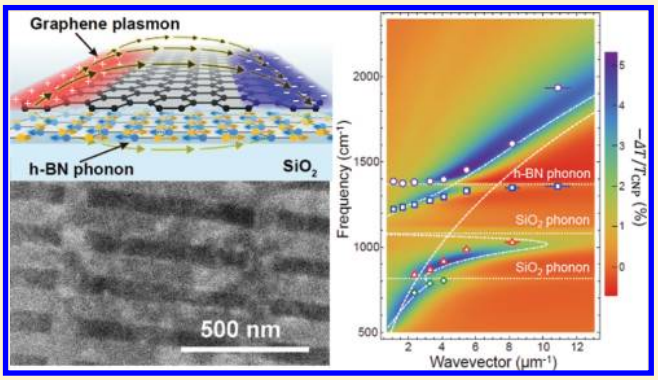

KEYWORDS: *Graphene, boron nitride, plasmonics, strong coupling, phonon-induced transparency, surface phonon plasmon polariton, plasmon phonon hybridization*

The extreme light localization that is achievable in plasmonic nanostructures enables plasmonic modes to couple to optical excitations in their local environments, such as molecular vibrations,[1] phonons,[2] or excitons.[3−5] This confined nature of plasmonic modes, which results in an increased local electric field strength, has yielded methods for sensing and modification of the local optical environment including enhanced molecular detection,[6−9] optically active chemical reactions,[10] selective cell apoptosis in carcinogenic tumors,[11] and enhancing solar cell efficiencies.[12] These investigations have motivated researchers to design structures that focus the electric field into smaller volumes to enhance the interaction strength and also to seek materials and structures that increase the lifetime of surface plasmon modes, which reduce plasmonic losses that inhibit coupling to nearby optical excitations. The ultimate limit for research in this area is to achieve complete spatial and temporal control of the plasmonic coupling interaction with the electronic and vibronic excitations of single molecules or atoms where cavity quantum electrodynamic effects can become significant. Reaching this limit requires the fabrication of plasmonic devices with mode volumes approaching the size of single molecules.

Graphene plasmonic nanostructures offer new opportunities to explore these coupling phenomena and to further increase the interaction strength.[13] In graphene, the plasmonic modes can be confined in extremely small volumes that have been demonstrated experimentally to be ∼10^7 times smaller than free space with wavelengths more than one hundred times shorter than the free space at mid-infrared frequencies.[14,15] In comparison, surface plasmons supported by normal metals typically display mode volumes that are 10^3 times smaller than freespace with similar damping.[15,16] Thus, it is expected that graphene plasmons should couple more strongly to their local environment than normal metal plasmons. Recent experiments performed on graphene devices on SiO_2[14,17] and SiC[18,19] substrates have shown that the graphene dispersion relation is indeed modified due to the substrate phonons with extra modes appearing due to plasmon-phonon coupling that have been described as surface-phonon-plasmon-polaritons, or SPPPs.[14] In those experiments, however, the substrates used were much thicker than the plasmonic wavelengths and thus did not test

Received: March 24, 2014
Revised: May 20, 2014

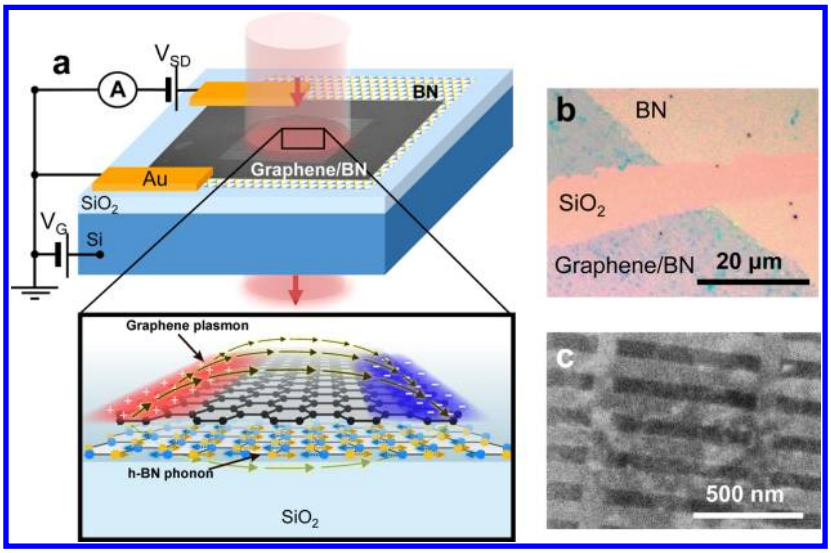

Figure 1. (a) Schematic of device measured and modeled in this paper. Graphene nanoresonators are fabricated on a monolayer h-BN sheet on a SiO_2(285 nm)/Si wafer. Gold contact pads are used to contact the graphene sheet and the Si wafer is used to apply an in situ backgate voltage (V_G). Zoom-in shows cartoon of graphene plasmon coupling to h-BN optical phonon. (b) Optical image of unpatterned area of device where both the graphene and h-BN monolayers have been mechanically removed. (c) Scanning electron microscope image of the 80 nm graphene nanoresonators (light regions).

whether the graphene plasmons were coupling to a large volume of phonons spread throughout the dielectric environment or only to the phonons in the immediate vicinity of the graphene sheet. Recently, experiments have been performed to investigate the coupling between graphene plasmons and thin layers of PMMA, showing that the PMMA phonon spectral signature can be enhanced through graphene plasmon coupling for PMMA layers as thin as 8 nm.[20] Here we fabricate graphene nanoresonator devices on a monolayer h-BN sheet in order to test the ability of graphene plasmons to couple to optical excitations that occupy an atomically thin slice of volume near the graphene. We find that the small mode volume of the graphene plasmons combined with the high oscillator strength of the h-BN phonons allows the two modes to strongly couple, forming two clearly separated hybridized SPPP modes that display an anticrossing behavior.

A schematic of our experimental device is shown in Figure 1. A monolayer h-BN sheet grown using chemical vapor deposition (CVD) on copper foil (Graphene Supermarket #CVD-2X1-BN) is transferred to a SiO_2 (285 nm)/Si wafer and a CVD-grown graphene sheet is subsequently transferred onto the h-BN. Nanoresonators are patterned into the graphene surface using 100 keV electron beam lithography in PMMA, followed by an oxygen plasma etch. Infrared spectroscopy analysis reveals that the h-BN layer is also degraded in the lithographed areas exposed to the oxygen plasma (see Supporting Information). The resonators are patterned into electronically continuous bar array patterns with widths ranging from 30 to 300 nm, and a 1:2 width-to-pitch ratio, as shown in Figure 1D. The dimensions of patterned nanoresonators are later precisely measured by using atomic force microscope (AFM). The Si layer was contacted and used as a back-gate electrode, and Cr(2 nm)/Au(100 nm) contacts were evaporated onto the nearby graphene surface such that the conductivity of the graphene could be monitored in situ. The charge neutral (zero carrier density) point was determined by the applied gate voltage that gave maximum resistance of the graphene sheet, and the carrier density at different gate voltages was determined by monitoring the cutoff energy of interband transitions in the graphene, which occurs at $2E_F$, where E_F is the graphene Fermi level.[21,22] As observed in previous work,[14] the charge neutral point is offset from zero gate voltage due to impurities introduced during the sample fabrication that hole-dope the sample (see Supporting Information). The device was then placed in a Fourier transform infrared spectroscopy (FTIR) microscope and measured in transmission mode with light polarized perpendicular to the nanoresonators. All graphene nanoresonator spectra were normalized relative to spectra taken with zero carrier density. For reference, a transmission spectrum was taken on a bare h-BN area of the sample, as shown at the bottom of Figure 2. As can be seen in the figure, the h-BN spectrum is flat except for a narrow (19 cm^{-1}) resonance near 1370 cm^{-1}, which has been assigned in previous studies as an in-plane optical phonon of the h-BN.[23]

Figure 2 illustrates the dependence of transmission spectra on graphene nanoresonator width at 1.0×10^{13} cm^{-2} carrier density. As can be seen in this figure, multiple features appear in the spectra, namely, two distinct sets of optical modes can be observed above and below 1200 cm^{-1}. The two modes below 1200 cm^{-1} have previously been observed in graphene plasmonic devices on SiO_2 and have been assigned to SPPP modes associated with two SiO_2 phonons.[14,17] The two modes above 1200 cm^{-1}, however, represent new optical features not observed in graphene/SiO_2 or graphene/SiC structures, which contained only a single dispersive mode above 1200 cm^{-1}. A close analysis of these two features reveals an anticrossing behavior near the 1370 cm^{-1} optical phonon energy of the h-BN with the lower (upper) mode approaching that energy for small (large) ribbon widths. Furthermore, there is a relative shift in intensity between the upper and lower modes as the ribbon width varies with the upper mode being more intense for small ribbon widths and vice versa. Significantly, the signal intensity between the two features drops nearly to zero for 80 nm resonator widths, when the two features have equivalent intensities.

dx.doi.org/10.1021/nl501096s | Nano Lett. XXXX, XXX, XXX−XXX

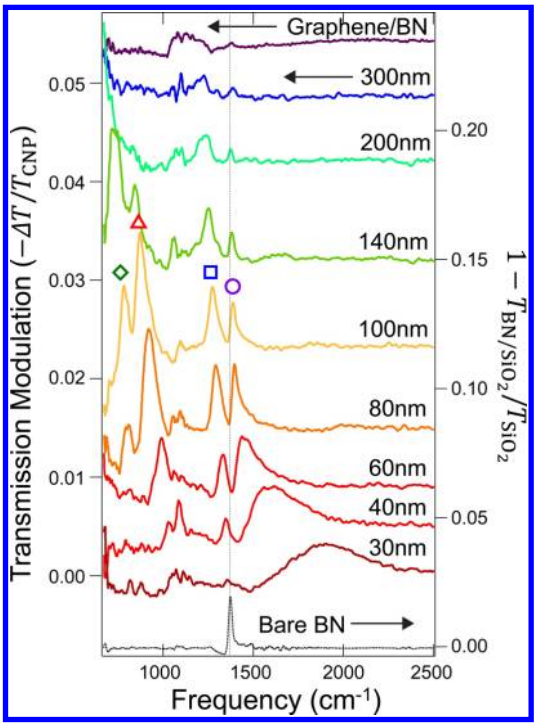

Figure 2. (Left axis) Normalized transmission spectra of graphene nanoresonators with widths varying from 30 to 300 nm, as well as transmission through the unpatterned graphene/h-BN sheet. Spectra are measured at carrier densities of 1.0×10^{13} cm^{-2} and normalized relative to zero carrier density. For 80 nm ribbons, the four different observable optical modes are labeled with the symbols used to indicate experimental data points in Figure 3. (Right axis, bottom spectrum) Infrared transmission of the bare monolayer h-BN on SiO_2 normalized relative to transmission through the SiO_2(285 nm)/Si wafer. The narrow (~19 cm^{-1}) peak that occurs at 1370 cm^{-1} has previously been assigned to an optical phonon in h-BN.[23] The dotted vertical line indicates this peak position as a reference for the other spectra.

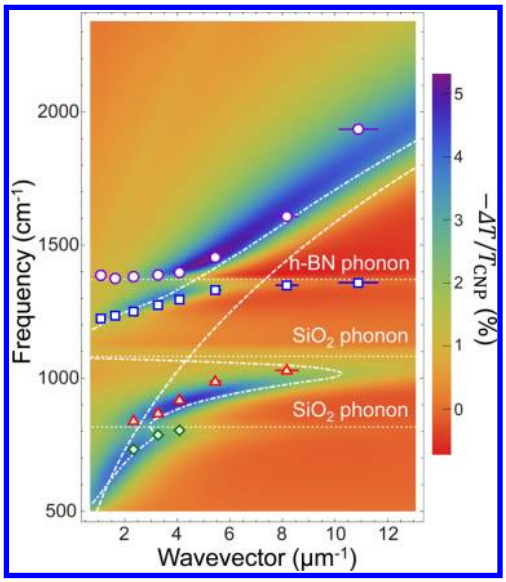

Figure 3. Calculated change in transmission for graphene/monolayer h-BN/SiO_2 nanoresonators of varying width at a carrier density of 1.0×10^{13} cm^{-2}, normalized relative to zero carrier density. The wavevector is determined by considering the ribbon width, W, as well as the phase of the plasmon scattering off the graphene ribbon edge, as described in the text. Experimental data is plotted as symbols indicating optical modes assigned in Figure 2. The error bars represent uncertainty in the resonator width that is obtained from AFM measurements. For small **k**-vectors (large resonators), this uncertainty is smaller than the symbol size. The dashed line indicates the theoretical dispersion for bare graphene plasmons, while the dash-dot line indicates the dispersion for graphene/SiO_2 The three horizontal dotted lines indicate the optical phonon energies of h-BN and SiO_2.

In order to better understand the characteristics of each mode, we calculate the transmission spectrum of graphene nanoresonators for various widths using a finite element method within a local random phase approximation.[24] Here, the in-plane dielectric function of monolayer h-BN is described using Lorentz oscillator model with parameters fitted from transmission measurement of the bare h-BN on SiO_2,[23] and its thickness is modeled to be 0.34 nm, which is the interlayer spacing of bulk h-BN (see Supporting Information for details). The scale-invariant plasmon phase shift upon reflection at the nanoresonator edges is calculated to be $\varphi \approx 0.35\pi$.[14] This implies that the plasmon wavevector $\mathbf{k}_p = (\pi - \varphi)/W$ for the first-order plasmon resonance with the width, W, extracted from AFM measurements. The resulting carrier-induced change in transmission is plotted in Figure 3 for varying wavevector and energy at 1.0×10^{13} cm^{-2} carrier density. The dispersion of the graphene/h-BN/SiO_2 nanoresonator optical modes can be observed in this plot as the maxima in the transmission modulation, $-\Delta T/T_{CNP}$. These features show a strong correspondence with the experimentally measured features with modes appearing above and below the h-BN optical phonon energy that display a clear anticrossing behavior.

The behavior displayed experimentally and theoretically in Figures 2 and 3 is indicative of a hybridization between the graphene plasmons modes and the h-BN optical phonon modes that creates two new SPPP modes with dispersion relations that are distinctly different from the original graphene plasmon dispersion (dashed line, Figure 3) as well as the graphene/SiO_2 dispersion (dashed-dotted line, Figure 3). This hybridization can be understood through an electromagnetically coupled oscillator model where the local polarization field created by lattice displacement in the h-BN exerts a force on the free carriers in the overlying graphene resonators via near field interaction, and likewise the polarization due to displaced carriers in the graphene exerts a force on the h-BN lattice. When this coupling becomes sufficiently strong, the lifetimes and the energies of the two constitutive optical modes can be significantly shifted and the resulting optical features are hybrid modes, or SPPPs. These new optical modes contain both plasmon-like and phonon-like character with the relative contribution of each constitutive mode dependent on the graphene ribbon width and carrier density. Recognizing that each spectrum displayed in Figure 2 shows the relative difference in transmission while varying the carrier density in graphene, the relative intensity of two resonances roughly indicates how much the graphene plasmon contributes to each hybrid SPPP mode. Therefore, we know that the upper (lower) SPPP mode is more plasmon-like for small (large) ribbon widths from the relative shift in peak intensity; for 80 nm graphene/h-BN resonators, the two modes are both equally plasmon-like and phonon-like. This behavior is consistent with the extracted dispersion properties of each mode shown in Figure 3.

In combination with the hybridization behavior described above, we observe a pronounced minimum in absorption near the h-BN phonon energy for 60, 80, and 100 nm resonators for

dx.doi.org/10.1021/nl501096s | Nano Lett. XXXX, XXX, XXX−XXX

which the bare graphene plasmon mode would typically overlap the h-BN phonon energy. We interpret this phenomenon as a classical, phonon-based analogue to electromagnetically induced transparency (EIT) experiments performed on atomic gases. In this description, it is observed that when the graphene plasmon mode is brought into resonance with the h-BN phonon, the polarizations of the two modes cancel each other out, creating a transparency window where no absorption occurs in the plasmonic modes. This mechanism can be explored theoretically, by plotting the electric field and polarization density profiles of 80 nm resonators at the upper and lower SPPP energies for 1.0×10^{13} cm^{-2} carrier density, as shown in Figure 4. These profiles show that at the peak

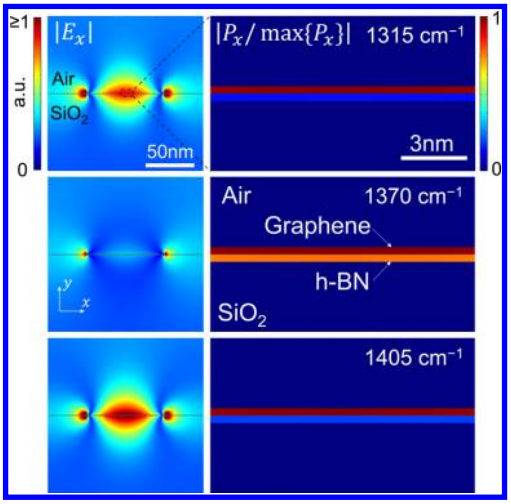

Figure 4. Theoretical electric field (E_x, left) and polarization density (P_x, right) profiles of 80 nm wide graphene nanoresonators at the lower SPPP (top), the transparency window (middle), and the upper SPPP (bottom) energies. The carrier concentration is assumed to be 1.0×10^{13}cm^{-2}.

absorption frequencies the polarization density is predominantly in the graphene sheet, and there is a large E-field that arises due to the optical resonance. In the transparency window, however, there is significant polarization density in the h-BN layer that acts to cancel out the polarization in the graphene sheet and results in a substantially weaker surrounding E-field. This indicates that the system has a small dipole moment and, therefore, weak optical coupling within the narrow frequency range where the graphene plasmon frequency matches the h-BN phonon frequency, thus creating the transparency window observed in our data.

The clearly separated resonance peaks also indicate that the coupling between graphene plasmons and the h-BN phonons enters a classical "strong-coupling" regime, where the associated electromagnetic interaction can fully transfer energy between the plasmon and phonon states before decaying via damping. This regime is characterized by a large splitting between the two hybridized modes, such that the minimum energy separation is more than the sum of the two line widths, and the spectral intensity between the two modes approaches zero.[25] For the experimental data shown here, the minimum splitting we observe between the two graphene/h-BN SPPPs is 100 cm^{-1} (for 80 nm resonators), which is more than the sum of the two associated peak widths of 25 and 55 cm^{-1}, indicating that the system is in a strong coupling regime.[25] This phenomena has been explored in conventional metal plasmonics experiments using molecular vibrations or dyes coupled to metallic plasmons.[3,4,7−9,26] In those experiments, however, a thick (>20 nm) layer of optically active material was required for strong coupling to be achieved. Here, we observe that the high confinement of graphene plasmons allows them to strongly couple to optical phonons in an atomically thin layer. In order to explore the limits of the graphene−h-BN coupling phenomena, we performed spectral simulations to investigate how the coupling strength varies as the spacing between 80 nm graphene ribbons and the h-BN layer is varied from 0 (direct contact) to 80 nm. As shown in Figure 5, both the splitting

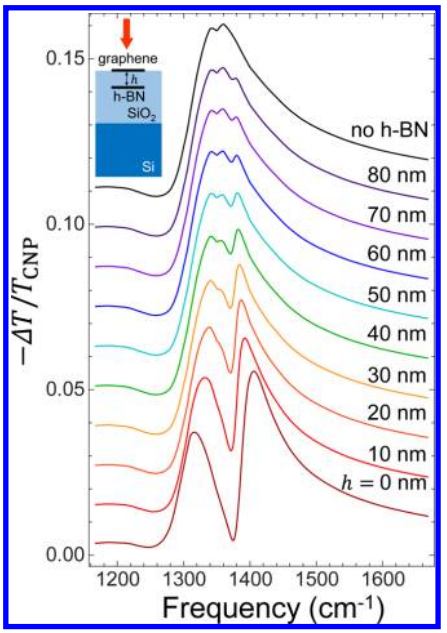

Figure 5. Calculated transmission spectra for 80 nm graphene/SiO_2/monolayer h-BN/SiO_2 ribbons as the first SiO_2 layer thickness is varied from zero (direct contact) to 80 nm in 10 nm increments. Spectra are for a carrier density of 1.0×10^{13} cm^{-2} and normalized relative to zero carrier density.

between two hybrid SPPP modes and the depth of the transparency window, which are indicatives of the coupling strength, rapidly decrease as the interlayer distance increases. When the layer spacing reaches 20 nm, the transparency depth is less than half of that when there is no interlayer spacing, and at an interlayer distance of 80 nm the coupling becomes so weak that the hybridization effects are barely observable. These simulations indicate that the large mode confinement of graphene plasmons restricts their range of interaction to just tens of nanometers from the graphene sheet.

In conclusion, this study shows that the high-field confinement of graphene plasmons allows for classical strong coupling to be observed between the graphene plasmons and the phonons of a monolayer h-BN sheet. The small volume of the h-BN sheet indicates that a very small number of optical excitations with large oscillator strengths are sufficient to achieve strong coupling to graphene plasmons, as long as the excitations are in the immediate vicinity of the graphene sheet. As the distance is increased, however, simulations show that this coupling phenomena rapidly decays with a characteristic length scale a few times shorter than the resonator width. This work indicates that graphene nanoresonators can serve as extremely sensitive probes of their local environments and

dx.doi.org/10.1021/nl501096s | Nano Lett. XXXX, XXX, XXX−XXX

opens the door for further investigations employing excitations of single or a few quanta interacting with the graphene plasmons.

■ ASSOCIATED CONTENT

Supporting Information

Section 1 shows details of the electromagnetic simulations and the model used to calculate the h-BN permittivity. Section 2 displays measurements and simulations at different carrier densities. Section 3 compares measurements of h-BN areas exposed and not exposed to the lithographic process used in this work. Section 4 shows how the graphene carrier density is determined in our experiment. This material is available free of charge via the Internet at http://pubs.acs.org.

■ AUTHOR INFORMATION

Corresponding Author

*E-mail: haa@caltech.edu.

Author Contributions

⊥V.W.B. and M.S.J. contributed equally.

Notes

The authors declare no competing financial interest.

■ ACKNOWLEDGMENTS

This work was supported by the Air Force Office of Scientific Research under MURI awards FA9550-12-1-0488 (V.W.B.), FA9550-12-1-0024 (S.K. and L.K.K.). M.S.J. and M.C. acknowledge support from the Global Frontier R&D Program on Center for Multiscale Energy Systems funded by the National Research Foundation under the Ministry of Science, ITC & Future Planning, Korea (2011-0031561, 2011-0031577). M.S.J. acknowledges a postdoctoral fellowship from the POSCO TJ Park Foundation. M.C.S. gratefully acknowledges graduate fellowship support from the Resnick Sustainability Institute at Caltech. The authors thank the Kavli Nanoscience Institute at Caltech for support of nanofabrication.

■ REFERENCES

(1) Moskovits, M. *Rev. Mod. Phys.* **1985**, *57* (3), 783−826.
(2) Hillenbrand, R.; Taubner, T.; Keilmann, F. *Nature* **2002**, *418* (6894), 159−162.
(3) Dintinger, J.; Klein, S.; Bustos, F.; Barnes, W. L.; Ebbesen, T. W. *Phys. Rev. B* **2005**, *71*, 035424.
(4) Sugawara, Y.; Kelf, T. A.; Baumberg, J. J.; Abdelsalam, M. E.; Bartlett, P. N. *Phys. Rev. Lett.* **2006**, *97*, 266808.
(5) Schlather, A. E.; Large, N.; Urban, A. S.; Nordlander, P.; Halas, N. J. *Nano Lett.* **2013**, *13* (7), 3281−3286.
(6) Brown, L. V.; Zhao, K.; King, N.; Sobhani, H.; Nordlander, P.; Halas, N. J. *J. Am. Chem. Soc.* **2013**, *135* (9), 3688−3695.
(7) Nau, D.; Seidel, A.; Orzekowsky, R. B.; Lee, S. H.; Deb, S.; Giessen, H. *Opt. Lett.* **2010**, *35* (18), 3150−3152.
(8) Neubrech, F.; Pucci, A.; Cornelius, T. W.; Karim, S.; Garcia-Etxarri, A.; Aizpurua, J. *Phys. Rev. Lett.* **2008**, *101*, 157403.
(9) Adato, R.; Yanik, A. A.; Amsden, J. J.; Kaplan, D. L.; Omenetto, F. G.; Hong, M. K.; Erramilli, S.; Altug, H. *Proc. Natl. Acad. Sci. U.S.A.* **2009**, *106* (46), 19227−19232.
(10) Schwartz, T.; Hutchison, J. A.; Genet, C.; Ebbesen, T. W. *Phys. Rev. Lett.* **2011**, *106*, 196405.
(11) Lal, S.; Clare, S. E.; Halas, N. J. *Acc. Chem. Res.* **2008**, *41* (12), 1842−1851.
(12) Atwater, H. A.; Polman, A. *Nat. Mater.* **2010**, *9* (3), 205−213.
(13) Koppens, F. H. L.; Chang, D. E.; de Abajo, F. J. G. *Nano Lett.* **2011**, *11* (8), 3370.
(14) Brar, V. W.; Jang, M. S.; Sherrott, M.; Lopez, J. J.; Atwater, H. A. *Nano Lett.* **2013**, *13* (6), 2541−2547.
(15) Jablan, M.; Buljan, H.; Soljacic, M. *Phys. Rev. B* **2009**, *80* (24), 245435.
(16) Maier, S. A. *Plasmonics: Fundamentals and Applications: Fundamentals and Applications*; Springer: New York, 2007.
(17) Yan, H.; Low, T.; Zhu, W.; Wu, Y.; Freitag, M.; Li, X.; Guinea, F.; Avouris, P.; Xia, F. *Nat. Photonics* **2013**, *7* (5), 394−399.
(18) Liu, Y.; Willis, R. F. *Phys. Rev. B* **2010**, *81*, 081102.
(19) Koch, R. J.; Seyller, T.; Schaefer, J. A. *Phys. Rev. B* **2010**, *82* (20), 201413.
(20) Li, Y.; Yan, H.; Farmer, D. B.; Meng, X.; Zhu, W.; Osgood, R. M.; Heinz, T. F.; Avouris, P. *Nano Lett.* **2014**, *14* (3), 1573−1577.
(21) Li, Z. Q.; Henriksen, E. A.; Jiang, Z.; Hao, Z.; Martin, M. C.; Kim, P.; Stormer, H. L.; Basov, D. N. *Nat. Phys.* **2008**, *4* (7), 532.
(22) Wang, F.; Zhang, Y. B.; Tian, C. S.; Girit, C.; Zettl, A.; Crommie, M.; Shen, Y. R. *Science* **2008**, *320* (5873), 206.
(23) Geick, R.; Perry, C. H.; Rupprecht, G. *Phys. Rev.* **1966**, *146* (2), 543−547.
(24) Falkovsky, L. A.; Varlamov, A. A. *Eur. Phys. J. B* **2007**, *56* (4), 281−284.
(25) Novotny, L. *Am. J. Phys.* **2010**, *78* (11), 1199−1202.
(26) Hakala, T. K.; Toppari, J. J.; Kuzyk, A.; Pettersson, M.; Tikkanen, H.; Kunttu, H.; Torma, P. *Phys. Rev. Lett.* **2009**, *103*, 053602.